Hindawi
Adsorption Science & Technology
Volume 2022, Article ID 8351796, 12 pages
https://doi.org/10.1155/2022/8351796

Research Article

Application of Mesopore-Activated Red Mud for Phosphorus Adsorption

Nguyen Dinh Trung,[1,2] Ning Ping,[3] and Ho Kim Dan[4,5]

[1]*Center for Analysis and Testing, Dalat University, Lam Dong, Vietnam*
[2]*Faculty of Chemistry and Environment, Dalat University, Lam Dong, Vietnam*
[3]*Faculty of Environmental Science and Engineering, Kunming University of Science and Technology, Kunming, 650500 Yunnan, China*
[4]*Optical Materials Research Group, Science and Technology Advanced Institute, Van Lang University, Ho Chi Minh City, Vietnam*
[5]*Faculty of Applied Technology, School of Engineering and Technology, Van Lang University, Ho Chi Minh City, Vietnam*

Correspondence should be addressed to Ho Kim Dan; hokimdan@vlu.edu.vn

Received 7 September 2022; Revised 2 November 2022; Accepted 25 November 2022; Published 13 December 2022

Academic Editor: Anjani Ravi Kiran Gollakota

In this paper, the mesopore-activated red mud (M-ARM) was prepared by treating red mud (RM) with acid under an ultrasonic batch and through heat treatment at 750 C. The surface area and adsorption average pore width of M-ARM were calculated and obtained values of 13.408 $m^2\ g^{-1}$ and 25.160 nm, respectively. Therefore, the maximum adsorption capacity of M-ARM for phosphorus was $200.85 \pm 1.66\ mg\ g^{-1}$ at 318 K and pH = 5. At a low initial concentration (75 mg L^{-1}), the phosphorus removal capacity by M-ARM material was up to 97.09 ± 0.15% at 313 K. With the temperature scales varying from 298 to 313 K, the values of Gibbs free energy change ($\Delta G\circ$) were negative and also vary from -37.47 to -36.68. The phosphorus adsorption process in an aqueous solution is spontaneous, and this adsorption process was exothermic with enthalpy change $\Delta H^o = -14.36$. From the results of investigations and calculations of thermodynamic values, kinetics, and adsorption capacity of materials, we can confirm that the materials in this study had a low-cost and potential material for applications to treat phosphorus-contaminated water. In addition, the adsorption kinetics of this material for phosphorus were also studied and discussed.

1. Introduction

In agricultural production, phosphorus (P) is a necessary nutrient for plant growth. However, if chemical fertilizers are not used properly, phosphorus will leach into the water, leading to harmful eutrophication of the aquatic [1]. When phosphorus levels are elevated in the water system, it stimulates the growth of cyanobacteria and degrades water quality. The phosphate concentrations in domestic wastewater are usually in the range of about 10 to 15 mg L^{-1} [2]. In natural water bodies, phosphate sources exist significantly in agricultural production, industrial production, household production, and several other fields. To reduce emissions of this nutrient to the aquatic environment, various techniques have been investigated to remove phosphate composition from wastewater before releasing them into the environment. There are several methods of phosphorus treatment such as biological removal, precipitation, adsorption, and ion exchange [2, 3]. Biotechnology is widely applied to remove phosphorus in water due to low operating costs, but the phosphorus removal efficiency is not satisfied with the requirements [4]. In recent years, many modern techniques and technologies have also been applied such as electrolysis and reverse osmosis membrane [5–7]. A few studies have also reported on the adsorption technology applied to remove organic phosphorus [6, 7]. In 2020, two projects at the Tan Rai Alumina Factory in Lam Dong province, Vietnam, exploited more than 1.4 million tons of alumina. Large quantities of red mud (RM) as a by-product of the plant are discharged daily. Therefore, the study of the application of

red mud in industrial production such as brick making, cement, and construction concrete, and their application in environmental treatment has also been of great interest to many people [5–9].

Nowadays, considerable attention has been paid to the application of low-cost, effective adsorbents from natural materials, or by-products from a variety of industries. RM is a sludge formed after the alkaline treatment of bauxite ore to produce alumina. RM often has a brick-red color because of the shape of iron compounds [8]. The main compositions of RM include fine particles that are metals in the form of oxides or hydroxides such as Al, Fe, Si, Ti, Ca, and Mg [9]. In recent times, there are many scientific publications on the applications of RM as an adsorbent to treat water contaminated with arsenic, heavy metals [10–13], dyes, antibiotics, and phenols [14–16]. The RM must be activated before being used as an adsorbent; the treatment of RM is to neutralize and remove some unnecessary compounds such as sand, gravel, sodium, and potassium. Normally, M-ARM is by methods such as acid treatment, heat treatment, and combined heat. The purpose of RM activation is to increase the surface area or porosity of the material [17]. The RM usually has a pH value of 10 to 13, so it needs to be treated before use. Several studies have reported the application of activated or inactivated RM to remove phosphorus from aqueous solutions. Some other studies have reported the RM activation method and the maximum adsorption capacity of RM for phosphorus. There are very few studies reported on the kinetics and thermodynamics of adsorption [18–20].

In this study, we focus on investigating and reporting the results of RM activated by HCl combined with ultrasonic batch and thermal activation. M-ARM is used as a material to remove phosphorus from an aqueous solution. Remarkably, we investigated their morphology and composition after activation, the influences of pH, contact times, adsorption isotherms, adsorption kinetics, and thermodynamics related to the adsorption process.

2. Experimental Details

2.1. Materials. The RM used in this study was provided by Tan Rai Alumina Factory in Lam Dong province, Vietnam. In the first step, the RM was dissolved in distilled water, the supernatant (emulsion mixture) was recovered, and the undissolved rock and gravel residue were removed. In the second step, the above emulsion mixture was centrifuged, and the residue (raw RM) was taken to the next step. The raw RM sample was first treated with 4 N hydrochloric acid, at a liquid/solid ratio of 20 mL/gram, for 24 h under stirring at 300 rpm and ultrasonic batch (Elma S300H). After the second step of treatment, we used distilled water several times to wash the residue until the pH reached neutral and continued drying at 100°C for 24 hours. In the third step, heat treatment was performed by placing the treated sample in a Nabertherm LT 15/12 furnace (Germany), calcined at 750°C for 5 h. The samples after heating, cooling, and grinding with agate mortar, M-ARM, were used for further study. The orthophosphate stock solution (1 g L^{-1}) was modulated by dissolving the KH_2PO_4 (Merk) salt into double distilled water. Phosphorus solutions in this study were prepared from the above stock solutions with different concentrations. From the P mass concentration can be calculated the orthophosphate content in the solutions.

2.2. Characterization of M-ARM Adsorbent. The elemental compositions of M-ARM were performed by the total reflection X-ray fluorescence spectrometry (TXRF) analysis on a TXRF S2 PICOFOX Bruker spectrometer using the gallium internal standard. To examine the surface area and the pore characteristics of M-ARM, the M-ARM adsorbent was analyzed by the Micromeritics-TriStar II 3020 3.02 (USA), Gas (Nitrogen) adsorption/desorption isotherms at 77 K. Scanning Electron Microscopy (SEM) images of M-ARM adsorbent was taken by JEOL JSM-6510LV (Japan) scanning electron microscopy.

2.3. Adsorption of Phosphorus by M-ARM. To study the batch adsorption process of phosphorus by M-ARM, the 500 mL Erlenmeyer flask contained 0.2 g M-ARM and 200 mL of the phosphorus solution, phosphorus in the solution has a concentration in the range of 75-250 mg L^{-1}. The reaction vessel was shaken at 300 rpm for 24 h. The adsorption process was studied in the temperature range from 298 to 313 Kelvin (K). HNO_3 0.01 N or NaOH 0.01 N was used to adjust pH. After adsorption, the mixture was centrifuged at 10000 rpm for 5 minutes. The supernatant was filtered through a 0.22 μm membrane using for phosphorus analysis. This procedure was adopted for all adsorption experiments, including pH effect, contact time, and evaluations of the isotherms. The phosphorus adsorption capacity by the M-ARM materials was calculated by the [21]:

$$q_e = \frac{V\,(C_i - C_e)}{M}, \tag{1}$$

where q_e is the phosphorus adsorption capacity by the M-ARM (in mg g^{-1} of M-ARM); V is the volume of solution (L) used; M is the mass (g) of M-ARM used for the phosphorus adsorption process; C_i and C_e are the phosphorus concentrations (mg L^{-1}) before and after the phosphorus adsorption processes, respectively.

2.3.1. Effect of Solution pH. We conducted the experiments by varying the pH value from 1 to 10, initial phosphorus concentration of 200 mg L^{-1}. All experiments were carried out according to Section 2.2, with a reaction time of 24 hours and a temperature of 298 K. After the phosphorus adsorption reaction was complete, the solution pH value was measured again.

2.3.2. Effect of Contact Times. To investigate the effects of contact times on phosphorus adsorption of M-ARM. We conduct experiments with the initial concentration of phosphorus ion of 200 mg L^{-1}, at pH = 5, and the survey time in the range of 30, 60, 90, 120, 150, and 180 minutes.

2.3.3. Effect of the Initial Phosphorus Concentrations. All experiments were performed under the procedure in Section

2.3; the initial phosphorus concentration was selected within the concentration range from 75 to 250 mg L^{-1}. The pH of the solutions was the optimum pH based on Section 2.3.1.

2.3.4. Adsorption Isotherm Study. Based on the study results in Section 2.3.2, the absorbance values of q_e corresponding to each initial concentration of phosphorus solutions were the basis for the study of the following isothermal adsorption processes from 298 to 313 K. The Langmuir adsorption and Freundlich adsorption were calculated as follows [21]:

$$q_e = \frac{q_m K_L C_e}{1 + K_L C_e}, \quad (2)$$

$$q_e = K_f C_e^{1/n}, \quad (3)$$

where q_e and C_e have been described in Formula (1); q_m is the maximum phosphorus adsorption capacity (in mg g^{-1}); K_L is the Langmuir constant (L mg^{-1}); n is the Freundlich constant; and Kf = $mg^{(1-1/n)}$ $L^{1/n}$/g.

2.3.5. Thermodynamic Studies. The adsorption of phosphorus by M-ARM has been performed in Section 2.3. With temperatures ranging from 298 to 313 K. The ΔG^0, ΔH^0, and ΔS^0 thermodynamic parameters were calculated by using the Van't Hoff equation.

2.4. Measurement of Phosphorus Concentration in Solutions before and after the Adsorption. Colorimetric photometry was a method used to analyze phosphorus with ammonium molybdate reagent, according to ISO 6878: 2004 standard method.

3. Results and Discussion

3.1. Characteristics of M-ARM

3.1.1. Surface Area (BET) and Pore Volume of M-ARM. Figure 1 shows the SEM image of RM treated only with HCl and without heat treatment. Figure 2 shows the SEM image of RM heated and treated at 750°C. When comparing the results in Figures 1 and 2, we can see that the RM materials after heat treatment have a smaller particle size and improved porosity.

To examine the surface area and the pore characteristics of M-ARM, N_2 adsorption/desorption measurements were performed and depicted in Figure 3. The isothermal plots of N_2 adsorption/desorption for the M-ARM show type IV isotherms. At low pressure, the adsorption process was monolayer, meanwhile at high-pressure adsorption occurred in multilayers.

The pore size distributions of M-ARM were calculated from adsorption and desorption data using the Barrett–Joyner–Halenda (BJH) model. The results in Figures 4(a) and 4(b) showed that most of the peaks in the range of 2 to 50 nm and the pore size of M-ARM were mostly mesopores with a pore width of 2 to 50 nm. Besides, the results of the physical properties analysis of M-ARM materials by the BET method were described in detail in Table 1.

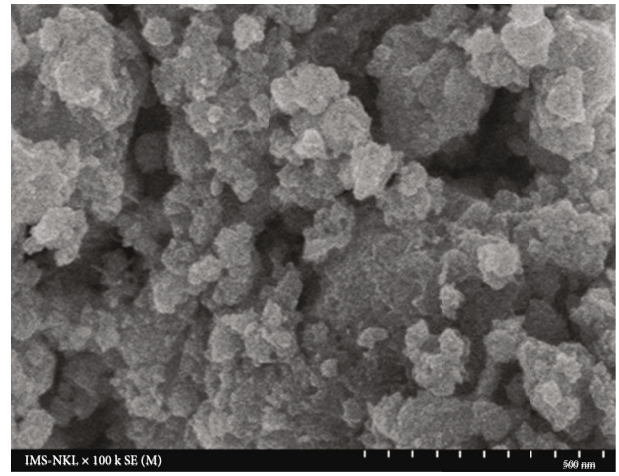

Figure 1: RM treated with 4 N hydrochloric acid.

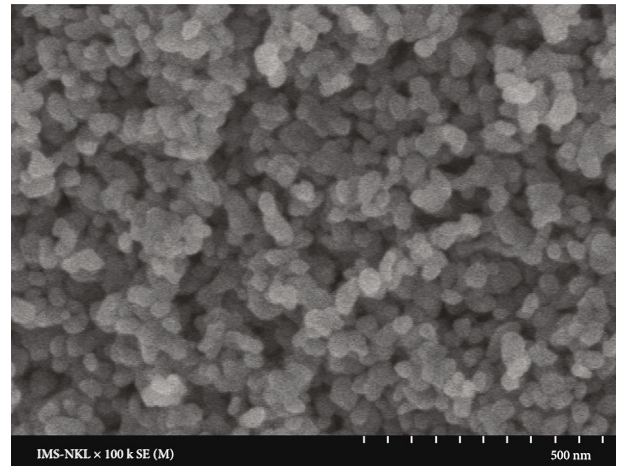

Figure 2: RM treated with 4 N hydrochloric acid and heat treatment at 750°C.

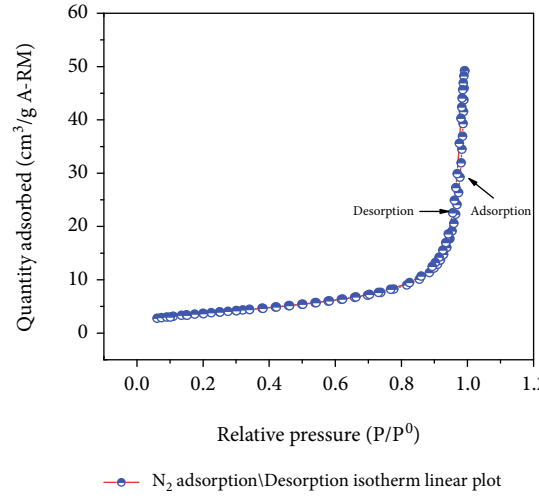

Figure 3: Isothermal plots of N_2 adsorption/desorption for the M-ARM.

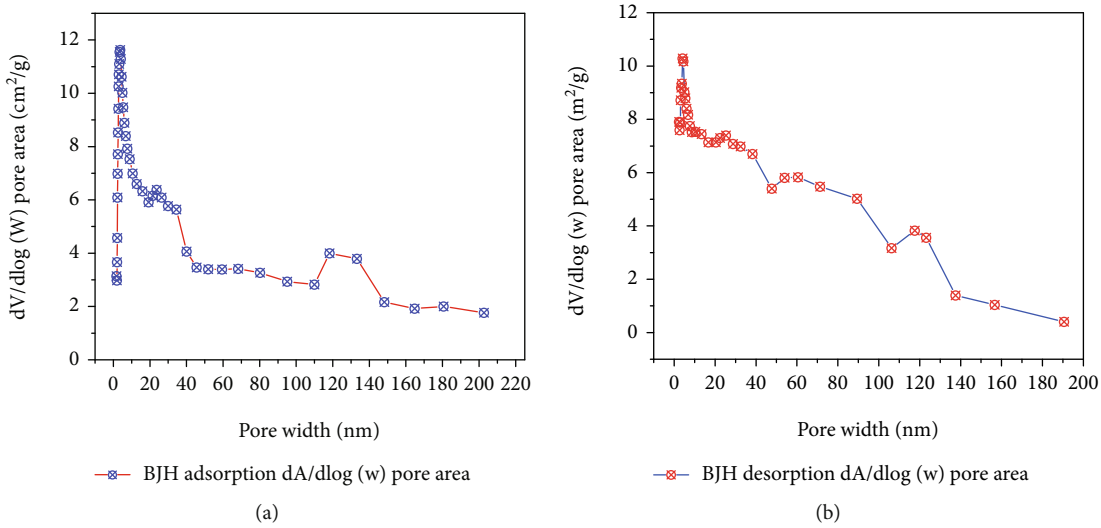

Figure 4: (a) BJH adsorption dV/dlog (W) pore area of M-ARM. (b) BJH desorption dV/dlog (W) pore area of M-ARM.

Table 1: The physicochemical characteristics of M-ARM.

BET surface area	13.408 m^2/g
BJH adsorption cumulative surface area of pores	12.163 m^2/g
BJH desorption cumulative surface area of pores	12.206 m^2/g
BJH adsorption cumulative volume of pores	0.076 cm^3/g
BJH adsorption average pore width (4 V/A)	25.160 nm
BJH desorption average pore width (4 V/A)	25.339 nm

3.1.2. The Elemental Composition of M-ARM Adsorbent. The elemental compositions of M-ARM material were performed and analyzed by the TXRF technique. The results of the TXRF analysis are described in Figure 5 and Table 2. When compared with the elemental compositions RM of different regions around the world shows that the main components are relatively similar, but the content of the elements is different. The results of this comparison are presented in Table 2.

3.2. Adsorption of Phosphorus by M-ARM

3.2.1. Effect of Solution pH. The results in Figure 6(a) showed that the phosphorus adsorbed by M-ARM materials was pH dependent. When the pH value changed from 1 to 2, this anion almost was not adsorbed because now, in solution, they exist in the form of H_3PO_4(aq) [27]. The maximum adsorption capacity of M-ARM materials for the phosphate anion was maximized when the pH reached a value between 4 and 5 due to at this pH value; the phosphate anion existed in solution in the form of $H_2PO_4^-$. When the pH value increased from 7 to 10, the maximum adsorption capacity decreased significantly. At this time, the OH^- radicals in the solution dominate, and phosphate anions exist in the solution in the form of HPO_4^{2-}, the OH^- competes for adsorption with HPO_4^{2-}[27]. Compared with previously published studies, such as (i) the paper published by Huang et al.'s research group in 2008 showed the best adsorption capacity of M-ARM at pH = 5.5 [20]; (ii) the work of Prajapati et al. suggested that the optimum pH value that RM adsorbs phosphorus is from 2 to 6 [18]; and (iii) the work of Li et al. reported that the best pH value for phosphorus adsorption by RM was 7 [19]. From the above statements, there are some differences which, in our opinion, may be due to different RM activation methods. To confirm, we need to survey a point of zero charges (PZCs) of M-ARM materials.

Therefore, we conducted the investigation and established the PZC of M-ARM in the aqueous adsorption. The results were shown in Figure 6(b). The PZC defined the M-ARM surface density of positive charge as equal to that of negative charge in the solution, which means $\Delta pH = pH_f - pH_i = 0$. Here, pH_i was the initial pH value, ranging from 1 to 10; pH_f was the pH value after the phosphate ions were absorbed by M-ARM. When $\Delta pH > 0$, the surface of M-ARM has a positive charge due to the surface of this adsorbent becoming protonated. When $\Delta pH < 0$, the surface of the adsorbent has a negative charge due to the surface of M-ARM becoming deprotonated [28].

When the pH_i value was from 1 to 2, $\Delta pH = 0$, adsorption did not occur; moreover, phosphorus in the solution exists in the form H_3PO_4(aq). When the value of pH_i changed from 4 to 10, $\Delta pH > 0$, the surface of the adsorbent has a positively charged due to the surface of M-ARM becoming protonated. When the value of pH_i increases from 7 to 10, ΔpH decreases rapidly, approaching zero. At pH_i = 5, ΔpH has the most positive value of +0.38; at this pH value, the maximum adsorption capacity of M-ARM materials for the phosphorus was maximized. In solution, phosphorus exists as negative anions; therefore, if the surface of the adsorbent has a positive charge, the phosphate anion adsorption process takes place more favorably (the opposite poles will attract one another). Interestingly, in this study, we determined a pH value of 5 was the best phosphorus

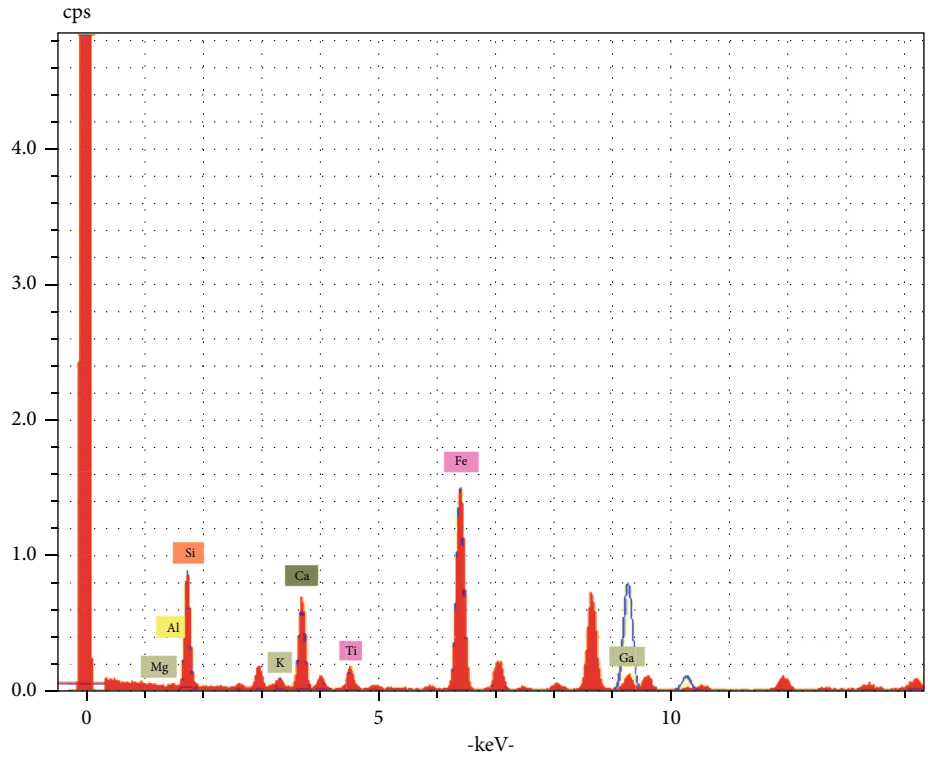

Figure 5: The components of the M-ARM were analyzed using TXRF.

adsorption condition of M-ARM. Thus, further studies were conducted at pH = 5.

3.2.2. Effect of Contact Time. We know that adsorption kinetics is an important parameter when investigating the adsorption process. Therefore, in this study, we also investigated the adsorption kinetics. Figure 7 described the adsorption kinetics of phosphorus by M-ARM in the form of pseudo-first-order (PFO) and pseudo-second-order (PSO) models. The results in Figure 6 showed that time affects the adsorption process. During the period from 30 to 90 min, the adsorption process took place rapidly, but when the time was 120 min, the adsorption reached equilibrium. When compared with the results published by Huang et al., there is not much difference [21].

The adsorption kinetics of the process was examined through two adsorption kinetic equations, PFO and PSO adsorptions. The PFO and PSO adsorption models were described by Trung et al. and Abd El-Rahman et al. according to the following formula [28, 29]:

$$\frac{dq_t}{dt} = K_1(q_e - q_t), \tag{4}$$

$$\frac{dq_t}{dt} = K_2(q_e - q_t)^2, \tag{5}$$

where q_e and q_t are the phosphorus amounts uptake per mass of M-ARM at equilibrium and at any time t (min), respectively; K_1 and K_2 (min^{-1}) are the constant rates of the PFO and PSO kinetic model, respectively. With the boundary conditions ($t = 0$, $q_t = 0$ and $t = t$, $q_e = q_t$), integrating Equations (4) and (5) lead to the following PFO and PSO nonlinearized forms:

$$q_t = q_e\left(1 - e^{-k_1 t}\right), \tag{6}$$

$$q_t = \frac{q_e^2 k_2 t}{q_e k_2 t + 1}. \tag{7}$$

Table 3 lists the parameters through the adsorption kinetic investigation. The value coefficient R^2 of PFO was 0.98, and the adsorption capacities calculated by this model were higher than the experimental value. The R^2 value of PSO was extremely high at 0.99 (see Figure 6), and the experimental data fitted the PSO model. Therefore, we can confirm that the PSO model was suitable for the description of phosphorus adsorption kinetics by M-ARM. The adsorption rate of the process depends on the phosphorus concentration gradient ($\triangle C$) for PFO, and ($\triangle C^2$) for PSO. Therefore, the adsorption rate of phosphorus by M-ARM was fast for 90 min; then, the adsorption rate of phosphorus by M-ARM slows down and the reaction reached adsorption equilibrium at 120 min.

3.2.3. Effect of the Initial Phosphorus Concentration at Temperatures from 298 to 318 K. The adsorption capacity of M-ARM materials for phosphorus corresponds to separate initial concentration ranges, different temperatures from 298-313 K. Experimental results were shown in Table 4; from the results show that when the phosphorus concentration

Table 2: Compare the main elemental compositions of RM from different regions.

Area	Elemental compositions of RM (wt%)								
	Fe_2O_3	Al_2O_3	SiO_2	TiO_2	Na_2O	CaO	MgO	K_2O	Refs.
M-ARM	45.94	19.95	6.80	3.10	—	12.60	0.10	0.50	This study
Queensland Alumina Ltd., Australia	34.05	25.45	17.06	4.90	2.74	3.69	1.86	0.20	[22]
Aluminium de Gréce S.A.	45.58	15.65	6.96	7.07	3.26	14.84	—	0.07	[23]
Eurallumina alumina plant, Italy	30.45	17.19	9.58	8.61	12.06	7.77	0.86	0.03	[24]
Shandong Aluminium Corporation, China	12.76	6.93	19.14	3.43	2.37	46.02	1.15	1.20	[25]
Seydiehir Aluminium plant, Konya, Turkey	35.73	23.29	12.08	4.08	7.40	2.81	0.76	0.28	[26]

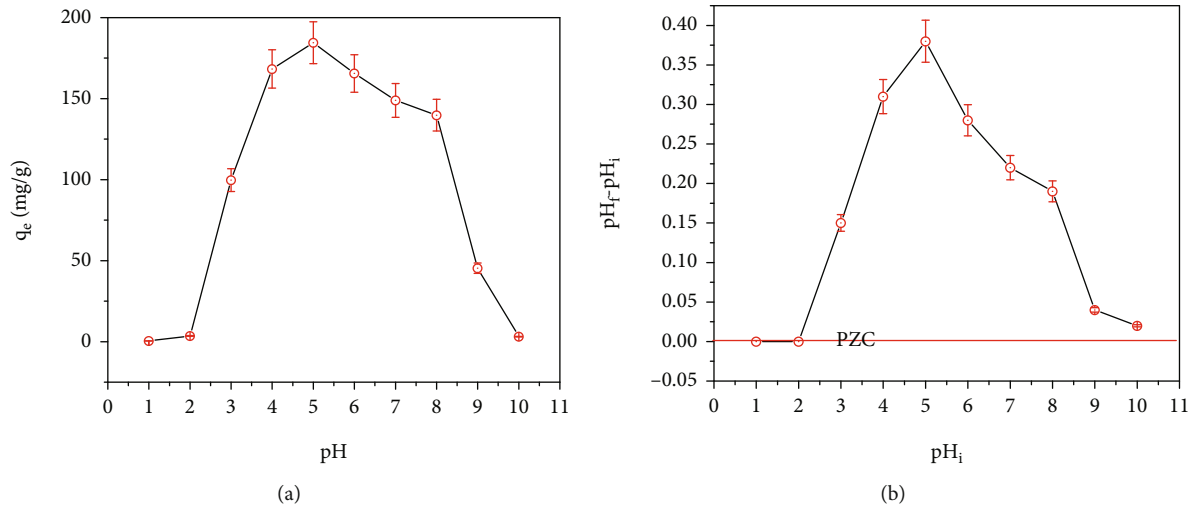

Figure 6: (a) Phosphorus adsorbed by M-ARM material at various initial pH conditions. (b) The plot of the variation in $\Delta pH = pH_f - pH_i$ with pH_i.

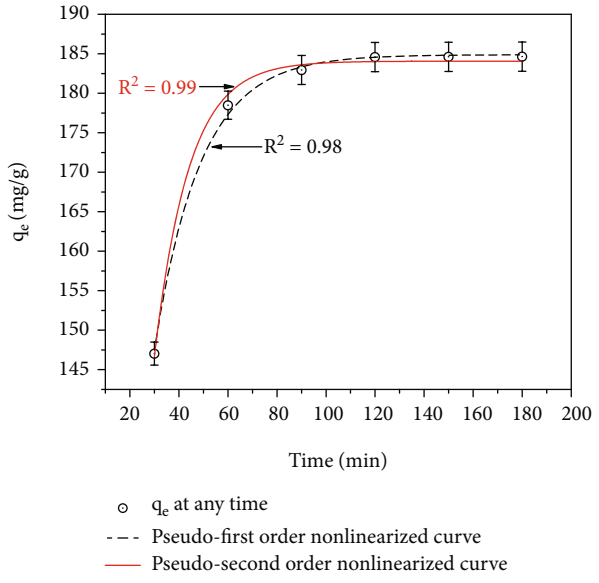

Figure 7: Adsorption kinetics of phosphorus by M-ARM in the form of PFO and PSO models.

Table 3: Parameters of PFO and PSO adsorption rate constants.

	PFO model		
	q_e (mg g^{-1})	K_1 (min^{-1})	R^2
Phosphorus	185.66 ± 3.62	0.05	0.98
PSO model			
	q_e (mg g^{-1})	K_2 (g/mg·min)	R^2
Phosphorus	184.53 ± 3.58	0.07	0.99

increases from 75-200 mg L^{-1}, the adsorption capacity also increases. However, when the initial concentration of phosphorus was higher than 230 mg L^{-1}, the adsorption capacity of the material did not increase any more for all 3 temperature ranges of 298, 303, and 313 K. The adsorption centers were filled, or the adsorption process of the material was saturated. When at a low initial concentration (75 mg L^{-1}), the phosphorus removal capacity by M-ARM material was up to 97.09 ± 0.15(%) at 313 K.

3.2.4. Adsorption Isotherm Study. Based on the experimental results presented in Table 4, Langmuir and Freundlich's isotherm adsorption models were applied to calculate the

Table 4: Phosphorus capacity of M-ARM at various initial phosphorus concentrations.

C_i (mg L^{-1})	q_e (mg g^{-1}) at 298 K	Phosphorus removal (%) at 298 K	q_e (mg g^{-1}) at 303 K	Phosphorus removal (%) at 303 K	q_e (mg g^{-1}) at 318 K	Phosphorus removal (%) at 313 K
75	73.78 ± 1.23	98.37 ± 0.13	73.38 ± 1.29	97.84 ± 0.14	72.82 ± 1.28	97.09 ± 0.13
100	98.12 ± 1.14	98.12 ± 0.15	97.72 ± 1.53	97.72 ± 0.15	97.18 ± 1.33	97.18 ± 0.12
120	116.95 ± 1.11	97.46 ± 0.11	116.54 ± 1.32	97.12 ± 0.15	116.03 ± 1.32	96.69 ± 0.12
145	139.82 ± 1.16	96.43 ± 0.16	139.41 ± 1.46	96.14 ± 0.16	138.87 ± 1.36	95.77 ± 0.13
170	160.06 ± 1.17	94.15 ± 0.10	159.85 ± 1.17	94.03 ± 0.11	159.24 ± 1.15	93.67 ± 0.17
200	184.59 ± 1.12	92.3 ± 0.08	184.28 ± 2.42	92.14 ± 0.13	183.74 ± 2.22	91.87 ± 0.12
230	184.79 ± 1.18	80.34 ± 0.19	184.29 ± 2.48	80.13 ± 0.19	183.9 ± 2.44	79.96 ± 0.21
250	189.59 ± 1.21	75.84 ± 0.23	184.38 ± 1.27	73.75 ± 0.21	183.94 ± 2.21	73.58 ± 0.19

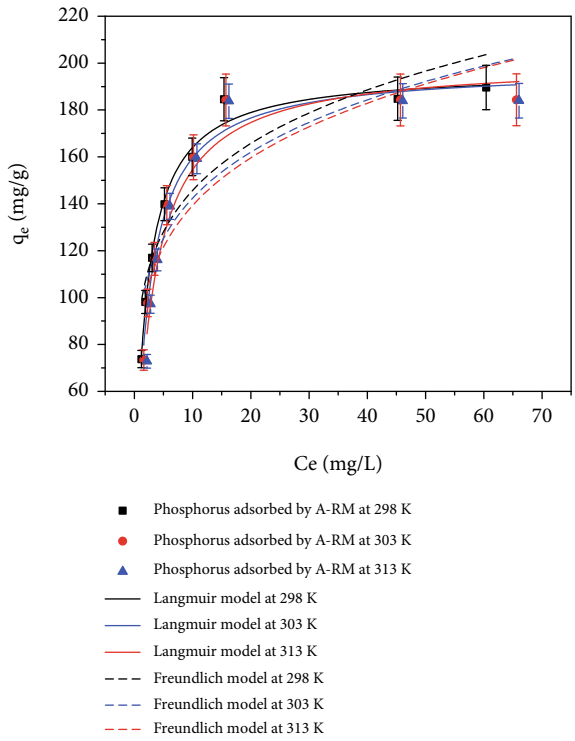

Figure 8: The relationship between C_e and q_e of phosphorus adsorption at pH = 5.

parameters of the adsorption process. Figure 8 showed the relationship between C_e and q_e of phosphorus adsorption at pH = 5, and temperature ranges of 298, 303, and 313 K. The calculation results obtained in Table 5 showed that when the temperature increases, the phosphorus adsorption capacity by M-ARM also increases. From the above analysis results, it was shown that the adsorption process of phosphorus by the M-ARM material was not only the process of monolayer adsorption on the surface but also by the pores of the material. Based on the Langmuir isotherm adsorption model, we can determine that the maximum adsorption capacity of M-ARM materials for phosphorus at 313 K was 200.85 ± 1.66 mg g^{-1}. The correlation coefficient (R^2) values

Table 5: Parameters of phosphorus adsorbed based of the Langmuir and Freundlich isotherm models.

(a)

Temperature (K)	Langmuir isotherm model		
	q_{max} (mg g^{-1})	K_L	R^2
298 K	196.84 ± 1.17	0.50	0.98
303 K	197.72 ± 1.62	0.42	0.97
318 K	200.85 ± 1.66	0.33	0.95

(b)

Temperature (K)	Freundlich isotherm model		
	K_f(mg$^{(1-1/n)}$ L$^{1/n}$/g)	1/n	R^2
298 K	37.30	0.18	0.83
303 K	36.01	0.18	0.77
318 K	35.46	0.20	0.75

of the Langmuir adsorption model under different temperature scales vary from 0.95 to 0.98, and the correlation coefficient (R^2) values of the Freundlich model were relatively low. Therefore, Langmuir isotherm can be used to describe the phosphorus adsorption process by M-ARM.

3.2.5. Thermodynamic Study. The adsorption thermodynamic parameters were determined through these parameters to confirm the phosphate ion adsorption feature by M-ARM materials, corresponding to conditions such as temperature and pH of the adsorption process. The Gibbs free energy change (ΔG^0), enthalpy change (ΔH^0), and entropy change (ΔS^0) are the basic thermodynamic parameters of the adsorption process that need investigating following equations:

$$\Delta G^0 = -R * T * \mathrm{Ln}K_C, \quad (8)$$

where $R = 8.314$ J mol^{-1} K^{-1} is the gas constant, T is the temperature (K), and K_C is the equilibrium constant. K_C

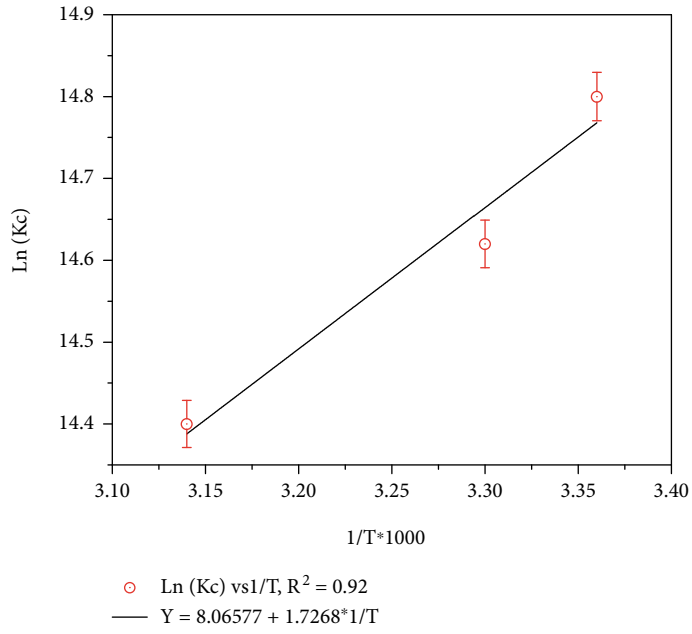

Figure 9: Plot of LnK_C vs. 1/T.

Table 6: Thermodynamic parameters for the adsorption of phosphorus by M-ARM.

T	K_L	K_C	LnK_C	$1/T^*1000$	ΔH^0 (kJ mol^{-1})	ΔS^0 (J mol^{-1})	ΔG^0 (kJ mol^{-1})
298 K	0.50	2687830	14.80	3.36	-14.36	67.06	-36.68
303 K	0.42	2246048	14.62	3.30			-36.84
318 K	0.33	1794937	14.40	3.14			-37.47

is calculated based on the K_L with the molar mass of $H_2PO_4^-$ = 96.99 g/mol [30]:

$$K_C = 96.99 * 1000 * 55.5 * K_L. \quad (9)$$

From the Van't Hoff equation, ΔG^0, ΔH^0, and ΔS^0 can be determined through the equation [31]:

$$\Delta G^0 = \Delta H^0 - T*\Delta S^0. \quad (10)$$

Clausius–Clapeyron equation describes the relationship between the equilibrium constant K_C and two parameters ΔH^0 and ΔS^0:

$$LnK_C = \frac{\Delta S^0}{R} - \frac{\Delta H^0}{R * T}. \quad (11)$$

The values of ΔH^0 and ΔS^0 were determined from the slope and intercept of the plot of LnK_C versus 1/T (see Figure 9). The results are presented in detail in Table 6.

From the calculation results in Table 6, the ΔG^0 value was negative for all temperature scales. So phosphorus was adsorbed by M-ARM material in a spontaneous process [32]. Positive entropy values ($\Delta S^0 = 67.06$) showed that phosphate ions were randomly concentrated on the surface of M-ARM materials. When the $\Delta H^0 = -14.36$ value was negative, the adsorption process was exothermic [33]; however, when the temperature of the process increased, the adsorption capacity increased (see Table 5). This phenomenon can be explained that as the temperature increased, the Brownian motion of the particles in the solution increased. Then, the phosphate ions easily got into the pores of the material. Yuan et al. [34] reported that phosphorus adsorption by dolomite mineral was the exothermic process, and Kalaitzidou et al. [35] reported phosphorus adsorption by iron oxyhydroxide material also gave the same result.

3.2.6. Comparing the Results in This Study with Other Studies. A comparison of the results of this study with the results of other studies is presented in Table 7; the M-ARM material in this study has a relatively high adsorption capacity for phosphorus. For RM, to be able to use them as phosphorus adsorbents, it is necessary to be activated. Depending on the activation method, they have different high or low maximum adsorption capacities, which were consistent with results reported by Yin et al. [36], Li et al. [19], and Liu et al. [37]. When compared with the results of Li et al. [19], the maximum adsorption capacity of M-ARM for phosphate was much higher. According to the report of Liu et al., when activating red mud by heat alone, the phosphate adsorption capacity was not high [37]. When

Table 7: Compared with the results of other studies.

Adsorbent	Initial concentration ($mg\,L^{-1}$)	Temperature (Kelvin)	pH	Times (min)	q_{max} ($mg\,g^{-1}$)	Refs.
Polypyrrole-modified RM	5-10	No mentioned	3-11	500	32.9	Yin et al. [36]
Raw RM					15.40	
RM700	0.31-3100	298	7	240	30.67	Li et al. [19]
RM0.25					30.70	
Acid-heat-activated RM	0-2500	298	7	120	202.9	Liu et al. [37]
Heat-activated RM					155.2	
Heat-treated RM	50-500	298	2-6	120	205.13	Prajapati et al. [18]
Modified RM with polypyrrole	1-25	298	2-5	Nt	195	Li et al. [38]
M-ARM	75-250	318	5	120	200.85 ± 1.66	This study

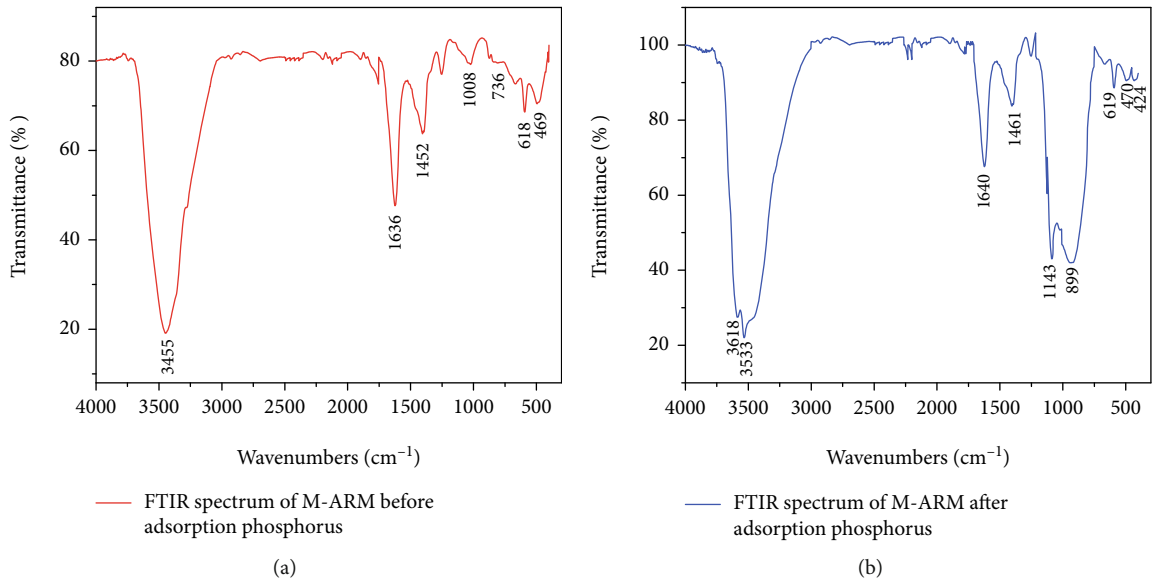

Figure 10: (a) FTIR spectrum of M-ARM material before phosphorus adsorption. (b) FTIR spectrum of M-ARM material after phosphorus adsorption.

combined with acid and heat treatment, the phosphorus adsorption capacity of the material increased significantly, which was also true of the results we reported in this manuscript. So, red mud used for phosphorus adsorption must be activated, depending on the activation method, it has a high or low adsorption capacity.

3.3. Mechanism of the Adsorption. The mechanism of phosphorus adsorption by M-ARM was complex and depends on both the composition and physical properties of the adsorbent. When adsorption occurs, the mechanism of phosphorus adsorption on M-ARM was not simple adsorption in surface complexation mode. There had been some reports that phosphates are adsorbed by gibbsite [16], goethite [39, 40], and calcite [41] groups, which were also the main constituents of M-ARM. In solution, when the $pH = 5.5$, the metal oxides Al_2O_3, Fe_2O_3, and CaO interacted with water molecules and became new hydrous metal oxide sites [40, 42]. These hydrous metal oxides are favorably complex with phosphorus on the surface or inside the pores of M-ARM material [17].

Figure 10(a) shows the FTIR spectrum of M-ARM material before phosphorus adsorption. From Figure 10(a), a narrow δ(HOH) band centered at $1636\,cm^{-1}$ was observed and there was a strong peak at $3445\,cm^{-1}$, which was the symmetrical stretching oscillation of ν(H-O-H) [43]. So the composition of this material contains water molecules, perhaps moisture in the air was adsorbed by this material. FTIR spectrum also has an obvious band centered at 469, 618, 736, and $1452\,cm^{-1}$ assigned to the ν(Fe-O), ν(Al-O), ν(Si-O), and

ν(Ca-O), respectively [42, 44]; in addition, a band centered at 1008 cm^{-1} could be identified as quartz and hematite phases which were typical of a red mud spectrum [45].

Figure 10(b) shows the FTIR spectrum of M-ARM material after phosphorus adsorption. From Figure 10(b) also appeared a narrow δ(HOH) band centered at 1636 cm^{-1}, and the peak of the symmetrical stretching oscillation of ν(H-O-H) has been shifted to 3550 cm^{-1} but with a stronger intensity than in Figure 10(b). There were some peaks compared to Figure 10(a) that had been shifted some units, such as ν(Ca-O) (1452 cm^{-1} shifted to 1461 cm^{-1}), ν(Fe-O) (469 cm^{-1} shifted to 470 cm-1), and ν(Al-O) (618 cm^{-1} shifted to 619 cm^{-1}). In Figure 10(b), some overlapping peaks appear at a strong intensity from 889 to 1134 cm^{-1}. Evidence obtained from ν(Fe-O-P) and ν(Al-O-P) showed bands centered at 889 and 1143 cm^{-1}, respectively [42], and a new δ(P-O-P) band was observed at 424 cm^{-1} [42]. Because in the composition of M-ARM, the calcium content was low, in Figure 10(b), two new peaks appeared, which were the main association of ν(Fe-O-P) and ν(Al-O-P). So, the mechanism of phosphorus adsorption by M-ARM materials was the complexation and deposition of $H_2PO_4^-$ on sites containing metal oxides such as iron and aluminium [46].

4. Conclusions

We have successfully prepared activated red mud, the mesopore-activated red mud (M-ARM) was prepared by treating red mud (RM) with acid HCl under ultrasonic batch and through heat treatment at 750°C. M-ARM has a surface area of 13.408 m^2/g and an adsorption average pore width of 25.160 nm. M-ARM has a maximum adsorption capacity for phosphorus of 200.85 ± 1.66 mg g^{-1} at pH = 5 and an adsorption temperature of 313 K. When at a low initial concentration (75 mg L^{-1}), the phosphorus removal capacity by M-ARM material was up to 97.09 ± 0.15% at 313 K. The PSO model was suitable to describe the adsorption kinetics of phosphorus by M-ARM; the reaction reached adsorption at 120 min. Langmuir model can be used to describe the phosphorus adsorption process by M-ARM. The $\Delta G\circ$ has negative values from -37.47 to -36.68, corresponding to the temperature scale from 298 to 313 K. From these results, it can be seen that the phosphorus adsorption process in an aqueous solution was spontaneous. $\Delta H^0 = -14.36$ was a negative value indicating that the adsorption process was exothermic. Therefore, M-ARM is a low-cost, easy-to-be-applied, readily available material, and a potential material for treating phosphorus-polluted water by adsorption.

Data Availability

The data used to support the findings of this study are available from the corresponding author upon request.

Conflicts of Interest

The authors declare that they have no conflicts of interest.

Acknowledgments

This research is funded by the Vietnam Ministry of Education and Training (MOE) under grant number B2020-DLA 01, and the authors are thankful to Dalat University and Van Lang University.

References

[1] H. Bacelo, A. M. A. Pintor, S. C. R. Santos, R. A. R. Boaventura, and C. M. S. Botelho, "Performance and prospects of different adsorbents for phosphorus uptake and recovery from water," *Chemical Engineering Journal*, vol. 381, article 122566, 2020.

[2] L. L. Blackall, G. Crocetti, A. M. Saunders, and P. L. Bond, "A review and update of the microbiology of enhanced biological phosphorus removal in wastewater treatment plants, Antonie Van Leeuwenhoek Int," *International Journal of Molecular Microbiology*, vol. 81, pp. 681–691, 2002.

[3] G. Akay, B. Keskinler, A. Cakici, and U. Danis, "Phosphate removal from water by red mud using crossflow microfiltration," *Water Research*, vol. 32, no. 3, pp. 717–726, 1998.

[4] Y. Luan, C. Qiu, Y. Li et al., "A highly packed biofilm reactor with cycle cleaning for the efficient treatment of rural wastewater," *Water*, vol. 13, no. 3, p. 369, 2021.

[5] E. Oguz, "Removal of phosphate from aqueous solution with blast furnace slag," *Journal of Hazardous Materials*, vol. 114, no. 1-3, pp. 131–137, 2004.

[6] X. G. Li, A. H. Elgarhy, M. E. Hassan, Y. Chen, G. Liu, and R. ElKorashey, "Removal of inorganic and organic phosphorus compounds from aqueous solution by ferrihydrite decoration onto graphene," *Environmental Monitoring and Assessment*, vol. 192, no. 6, p. 410, 2020.

[7] J. T. Bunce, E. N. Dam, I. D. Ofiteru, A. Moore, and D. W. Graham, "A review of phosphorus removal technologies and their applicability to small-scale domestic wastewater treatment systems," *Frontiers in Environmental Science*, vol. 6, pp. 1–15, 2018.

[8] M. Wang and X. Liu, "Applications of red mud as an environmental remediation material: a review," *Journal of Hazardous Materials*, vol. 408, article 124420, 2021.

[9] S. Kumar, R. Kumar, and A. Bandopadhyay, "Innovative methodologies for the utilisation of wastes from metallurgical and allied industries," *Resources, Conservation and Recycling*, vol. 48, no. 4, pp. 301–314, 2006.

[10] W. Wu, Z. Chen, Y. Huang et al., "Red mud for the efficient adsorption of U(VI) from aqueous solution: influence of calcination on performance and mechanism," *Journal of Hazardous Materials*, vol. 409, article 124925, 2021.

[11] Z. Lu, X. Qi, X. Zhu, X. Li, K. Li, and H. Wang, "Highly effective remediation of high-arsenic wastewater using red mud through formation of $AlAsO_4$@silicate precipitate," *Environmental Pollution*, vol. 287, article 117484, 2021.

[12] F. Lyu, S. Niu, L. Wang, R. Liu, W. Sun, and D. He, "Efficient removal of Pb(II) ions from aqueous solution by modified red mud," *Journal of Hazardous Materials*, vol. 406, article 124678, 2021.

[13] Z. Wang, P. Liao, X. He, P. Wan, B. Hua, and B. Deng, "Enhanced arsenic removal from water by mass re-equilibrium: kinetics and performance evaluation in a binary-adsorbent system," *Water Research*, vol. 190, article 116676, 2021.

[14] S. Aydin, M. E. Aydin, F. Beduk, and A. Ulvi, "Removal of antibiotics from aqueous solution by using magnetic Fe_3O_4/red mud-nanoparticles," *Science of the Total Environment*, vol. 670, pp. 539–546, 2019.

[15] S. R. Thakare, J. Thakare, P. T. Kosankar, and M. R. Pal, "A chief, industrial waste, activated red mud for subtraction of methylene blue dye from environment," *Materials Today: Proceedings*, vol. 29, no. 3, pp. 822–827, 2020.

[16] A. Tor, Y. Cengeloglu, and M. Ersoz, "Increasing the phenol adsorption capacity of neutralized red mud by application of acid activation procedure," *Desalination*, vol. 242, no. 1-3, pp. 19–28, 2009.

[17] J. Y. Lin, M. Kim, D. Li, H. Kim, and C. Huang, "The removal of phosphate by thermally treated red mud from water: the effect of surface chemistry on phosphate immobilization," *Chemosphere*, vol. 247, article 125867, 2020.

[18] S. S. Prajapati, P. A. M. Najar, and V. M. Tangde, "Removal of phosphate using red mud: an environmentally hazardous waste by- product of alumina industry," *Advances in Chemical Physics*, vol. 2016, pp. 1–9, 2016.

[19] Y. Li, C. Liu, Z. Luan et al., "Phosphate removal from aqueous solutions using raw and activated red mud and fly ash," *Journal of Hazardous Materials*, vol. 137, no. 1, pp. 374–383, 2006.

[20] W. Huang, S. Wang, Z. Zhu et al., "Phosphate removal from wastewater using red mud," *Journal of Hazardous Materials*, vol. 158, no. 1, pp. 35–42, 2008.

[21] N. Ayawei, A. N. Ebelegi, and D. Wankasi, "Modelling and interpretation of adsorption isotherms," *Journal of Chemistry*, vol. 2017, Article ID 3039817, 11 pages, 2017.

[22] H. Genç-Fuhrman, H. Bregnhøj, and D. McConchie, "Arsenate removal from water using sand-red mud columns," *Water Research*, vol. 39, no. 13, pp. 2944–2954, 2005.

[23] K. Komnitsas, G. Bartzas, and I. Paspaliaris, "Efficiency of limestone and red mud barriers: laboratory column studies," *Minerals Engineering*, vol. 17, no. 2, pp. 183–194, 2004.

[24] A. F. Bertocchi, M. Ghiani, R. Peretti, and A. Zucca, "Red mud and fly ash for remediation of mine sites contaminated with as, cd, cu, Pb and Zn," *Journal of Hazardous Materials*, vol. 134, no. 1-3, pp. 112–119, 2006.

[25] P. Li, D. E. Miser, S. Rabiei, R. T. Yadav, and M. R. Hajaligol, "The removal of carbon monoxide by iron oxide nanoparticles," *Applied Catalysis B: Environmental*, vol. 43, no. 2, pp. 151–162, 2003.

[26] N. Yalçın and V. Sevinç, "Utilization of bauxite waste in ceramic glazes," *Ceramics International*, vol. 26, no. 5, pp. 485–493, 2000.

[27] D. S. Gouveia, A. H. A. Bressiani, and J. C. Bressiani, "Phosphoric acid rate addition effect in the hydroxyapatite synthesis by neutralization method," *Materials Science Forum*, vol. 530-531, pp. 593–598, 2006.

[28] N. D. Trung, N. Ping, and H. K. Dan, "Synthesis, characterization, and the effectiveness of cobalt hexacyanoferrate nanoparticles in Cs^+ adsorbent application," *Journal Nanotechnology for Environmental Engineering*, vol. 7, no. 4, pp. 893–905, 2022.

[29] N. D. Trung, N. Ping, L.T.H. Lan, and H. K. Dan, "Synthesis, characterization, and caesium adsorbent application of trigonal zinc hexacyanoferrate (II) nanoparticles," *Journal of Environmental Chemical Engineering*, vol. 9, no. 6, article 106772, 2021.

[30] X. Zhou and X. Zhou, "The unit problem in the thermodynamic calculation of adsorption using the Langmuir equation," *Chemical Engineering Communications*, vol. 201, no. 11, pp. 1459–1467, 2014.

[31] N. K. Mondal, A. Samanta, S. Dutta, and S. Chattoraj, "Optimization of Cr(VI) biosorption onto _Aspergillus niger_ using 3-level Box- Behnken design: equilibrium, kinetic, thermodynamic and regeneration studies," *Journal, Genetic Engineering & Biotechnology*, vol. 15, no. 1, pp. 151–160, 2017.

[32] K. M. A. El-Rahman, A. M. El-Kamash, M. R. El-Sourougy, and N. M. Abdel-Moniem, "Thermodynamic modeling for the removal of Cs^+, Sr^{2+}, $^{Ca2+and}$ Mg2+ions from aqueous waste solutions using zeolite A," *Journal of Radioanalytical and Nuclear Chemistry*, vol. 268, no. 2, pp. 221–230, 2006.

[33] D. C. Emeniru, N. John, and J. Ikirigo, "Perspective view on sorption thermodynamics: basic dye uptake on southern Nigerian clay," *European Scientific Journal*, vol. 13, no. 18, pp. 355–372, 2017.

[34] X. Yuan, W. Xia, J. An, J. Yin, J. X. Zhou, and W. Yang, "Kinetic and thermodynamic studies on the phosphate adsorption removal by dolomite mineral," *Journal of Chemistry*, vol. 2015, Article ID 853105, 8 pages, 2015.

[35] K. Kalaitzidou, A. Zouboulis, and M. Mitrakas, "Thermodynamic study of phosphate adsorption and removal from water using iron oxyhydroxides," *Water*, vol. 14, no. 7, p. 1163, 2022.

[36] Y. Yin, G. Xu, Y. Xu et al., "Adsorption of inorganic and organic phosphorus onto polypyrrole modified red mud: evidence from batch and column experiments," *Chemosphere*, vol. 286, no. 3, article 131862, 2022.

[37] C. Liu, Y. Li, Z. Luan, Z. Chen, Z. Zhang, and Z. Jia, "Adsorption removal of phosphate from aqueous solution by active red mud," *Journal of Environmental Sciences*, vol. 19, no. 10, pp. 1166–1170, 2007.

[38] X. Li, M. Ji, L. D. Nghiem et al., "A novel red mud adsorbent for phosphorus and diclofenac removal from wastewater," *Journal of Molecular Liquids*, vol. 303, article 112286, 2020.

[39] A. Ler and R. Stanforth, "Evidence for surface precipitation of phosphate on goethite," *Environmental Science & Technology*, vol. 37, no. 12, pp. 2694–2700, 2003.

[40] L. Li and R. Stanforth, "Distinguishing adsorption and surface precipitation of phosphate on goethite (α-FeOOH)," *Journal of Colloid and Interface Science*, vol. 230, no. 1, pp. 12–21, 2000.

[41] I. Perassi and L. Borgnino, "Adsorption and surface precipitation of phosphate onto $CaCO_3$-montmorillonite: effect of pH, ionic strength and competition with humic acid," *Geoderma*, vol. 232-234, pp. 600–608, 2014.

[42] S. V. Stefanovsky, O. I. Stefanovsky, M. B. Remizov, E. A. Belanova, P. V. Kozlov, and B. F. Myasoedov, "FTIR and Mossbauer spectroscopic study of sodium-aluminum-iron phosphate glassy materials for high level waste immobilization," *Journal of Nuclear Materials*, vol. 466, pp. 142–149, 2015.

[43] S. Singh, M. U. Aswath, R. Das Biswas, R. V. Ranganath, and B. Sahoo, "Role of iron in the enhanced reactivity of pulverized red mud: analysis by Mossbauer spectroscopy and FTIR spectroscopy," *Case Studies in Construction Materials*, vol. 11, article e00266, 2019.

[44] M. M. Al Bakri Abdullah, K. Hussin, M. Bnhussain, K. N. Ismail, Z. Yahya, and R. A. Razak, "Fly ash-based geopolymer lightweight concrete using foaming agent,"

International Journal of Molecular Sciences, vol. 13, no. 6, pp. 7186–7198, 2012.

[45] D. Dodoo-Arhin, D. S. Konadu, E. Annan, F. P. Buabeng, and A. Yaya, "Fabrication and characterization of Ghanaian bauxite red mud-clay composite bricks for construction applications," *American Journal of Materials Science*, vol. 3, pp. 110–119, 2013.

[46] H. Wu, J. Wang, E. Duan, W. Hu, Y. Dong, and G. Zhang, "Phosphorus removal by adsorbent based on poly-aluminum chloride sludge," *Water Science and Engineering*, vol. 13, no. 3, pp. 193–201, 2020.